IV International Conference on Computational Methods for Coupled Problems in Science and Engineering
COUPLED PROBLEMS 2011
M. Papadrakakis, E. Oñate and B. Schrefler (Eds)

AN OPTIMIZED RETURN MAPPING ALGORITHM FOR THE BARCELONA BASIC MODEL

M. PERTL*, M. HOFMANN† AND G. HOFSTETTER*

* Unit for Strength of Materials and Structural Analysis
Institute for Basic Sciences in Civil Engineering
University of Innsbruck, Technikerstraße 13, 6020 Innsbruck, Austria
e-mail: michael.pertl@uibk.ac.at, web page: http://www.uibk.ac.at/bft

† ALPINE BeMo Tunneling GmbH
Bernhard-Höfel-Straße 11, 6020 Innsbruck, Austria
e-mail: matthias.hofmann@alpine-bemo.com, web page: http://www.bemo.net/

Key words: partially saturated soil, stress update algorithm, embankment dam

Abstract. For the most well-known constitutive model for partially saturated soils, the Barcelona Basic Model, an optimized return mapping algorithm is proposed, which is characterized by analytical integration of the hardening law and by solving only a nonlinear scalar equation at the integration point level. To investigate the performance of the proposed algorithm several implicit and explicit stress update algorithms are compared at the integration point level. Finally, the proposed stress update algorithm is applied to a 2D solid-fluid coupled numerical simulation of water flow through a homogeneous embankment dam.

1 INTRODUCTION

The development of constitutive models for partially saturated soil and the implementation into FE-programs are ongoing research topics. The latter requires selection of a suitable stress update algorithm. In addition to accuracy, robustness and efficiency of the employed stress update algorithm play a decisive role especially for large-scale FE-analyses. This is the motivation for developing an optimized return mapping algorithm for the most well-known constitutive model for partially saturated soils, the Barcelona Basic Model (BBM). In the pioneering work [1] basic concepts of modeling the behavior of partially saturated soils were introduced, e. g. the application of two independent stress parameters, consisting in the particular case of net stress and matric suction. The original version of the BBM was developed further by e. g. [7, 14, 2]. However, it is employed here in its original version, because the latter was agreed as the basis for extensive benchmark activities within the framework of the MUSE network [9].

Following the ideas of [5] the proposed algorithm is derived from the general formulation of the return mapping algorithm [13]. Whereas the latter requires solving a system of several nonlinear equations at the integration point level, the former is characterized by analytical integration of the hardening law and by solving only a nonlinear scalar equation at the integration point level.

To investigate the performance of the proposed algorithm several stress update algorithms are compared at the integration point level. This is done on the basis of two sets of material parameters for the BBM by prescribing different volumetric and deviatoric strain increments at constant matric suction. The investigated stress update algorithms include both implicit and explicit integration schemes. The latter include a forward Euler integration scheme and a semi-explicit integration algorithm [10]. The Richardson extrapolation method, described in [3], is used as the basis for sub-stepping with error control, which is an essential ingredient especially of explicit stress update algorithms. Moreover, enhancements of implicit integration methods with sub-stepping and error control techniques are investigated. In addition, a fifth-order Runge–Kutta stress update algorithm with error control is included in this investigation [4].

Finally, the proposed stress update algorithm is applied to a 2D solid-fluid coupled numerical simulation of water flow through a homogeneous embankment dam. The governing equations of the finite element formulation are based on a three-phase model for partially saturated soils, see e. g. [8]. Since in such structural analyses various hydro-mechanical loading conditions are encountered at different integrations points, the robustness and efficiency of the proposed stress update algorithm can be demonstrated.

2 THE BARCELONA BASIC MODEL

The BBM is formulated in terms of the net stress tensor $\boldsymbol{\sigma}''$ and the matric suction p^c. The net stress

$$\boldsymbol{\sigma}'' = \boldsymbol{\sigma} - p^a \mathbf{I} \tag{1}$$

is the total stress $\boldsymbol{\sigma}$ in excess of the pore air pressure p^a, and the matric suction

$$p^c = p^a - p^w \tag{2}$$

is the difference between the air pressure p^a and the water pressure p^w. For stress states located within the elastic domain, enclosed by the yield surface, the elastic volumetric and deviatoric strain rates are given as

$$\dot{\varepsilon}_v^e = \frac{\kappa}{1+e}\frac{\dot{p}''}{p''} + \frac{\kappa_s}{1+e}\frac{\dot{p}^c}{p^c + p_{atm}} \ , \quad \dot{e}_{ij}^e = \frac{\dot{s}_{ij}}{2G} \ , \tag{3}$$

with the material parameters κ and κ_s, representing the elastic stiffness for changes of the mean net pressure $p'' = (\boldsymbol{\sigma}'' : \mathbf{I})/3$ and for changes of the matric suction p^c, respectively. e, p_{atm}, $\dot{s}_{ij}$ and G denote the void ratio, the atmospheric air pressure, the deviatoric stress rate and the shear modulus, respectively. It follows from (3_1) that the elastic volumetric

strain rate $\dot{\varepsilon}_v^e$ depends on both the mean net pressure p'' and the matric suction p^c. Within the elastic domain the stress point (p'', e) lies on the unloading-reloading line (URL) with slope κ. For isotropic plastic conditions it lies on the isotropic compression line (ICL) with the suction-dependent slope

$$\lambda(p^c) = \lambda(0)\ \left[(1-r)\, e^{-\beta\, p^c} + r\right]\ . \tag{4}$$

$\lambda(p^c)$ describes the soil stiffness during plastic loading in a hydrostatic test for a given matric suction p^c in terms of the respective stiffness $\lambda(0)$ at saturated conditions and the material parameters r and β.

The intersection point of the URL and the ICL is denoted as the preconsolidation pressure p_0''. The ICL is defined by the slope $\lambda(p^c)$ and the void ratio $e = N(p^c) - 1$ at $p'' = 1$ with $N(p^c)$ denoting the respective specific volume. From the volumetric behavior of the BBM follows

$$e = N(p^c) - 1 - \lambda(p^c) \ln\left(\frac{p_0''}{1}\right) + \kappa \ln\left(\frac{p_0''}{p''}\right)\ , \tag{5}$$

from which

$$p_0'' = \exp\left(\frac{-N(p^c) + 1 + e}{\kappa - \lambda(p^c)}\right) p''^{\frac{\kappa}{\kappa - \lambda(p^c)}} \tag{6}$$

is obtained. The yield surface is defined as

$$f = J_2 - \frac{M^2}{3}\,(p'' + p_s'')\,(p_0'' - p'') \tag{7}$$

with the second invariant of the deviatoric stress tensor $J_2 = s_{ij}s_{ij}/2$ and

$$p_s''(p^c) = k_s p^c\ , \quad p_0'' = p_{ref}'' \left(\frac{(p_0'')^*}{p_{ref}''}\right)^{\frac{\lambda(0)-\kappa}{\lambda(p^c)-\kappa}}\ . \tag{8}$$

In (7) M defines the slope of the critical state line. p_s'' and p_0'' both depend on the matric suction according to (8). For negative values of p'' the intersection of the yield surface (7) with the plane $J_2 = 0$ is given by p_s'' according to (8_1) with the material parameter k_s describing the increase in cohesion due to the matric suction. The preconsolidation pressure p_0'' and the one for saturated conditions $(p_0'')^*$ are located on the so called loading collapse yield curve (LC curve) according to (8_2). This curve is the intersection of the yield surface with the plane $J_2 = 0$ for positive values of p''. Here, p_{ref}'' serves as a reference pressure such that for $(p_0'')^* = p_{ref}''$ (8_2) degenerates to $p_0'' = p_{ref}'' = \text{const}$.

The plastic strain rate is determined from the non-associated flow rule

$$\dot{\varepsilon}_{ij}^p = \dot{\gamma}\frac{\partial g}{\partial \sigma_{ij}''} \tag{9}$$

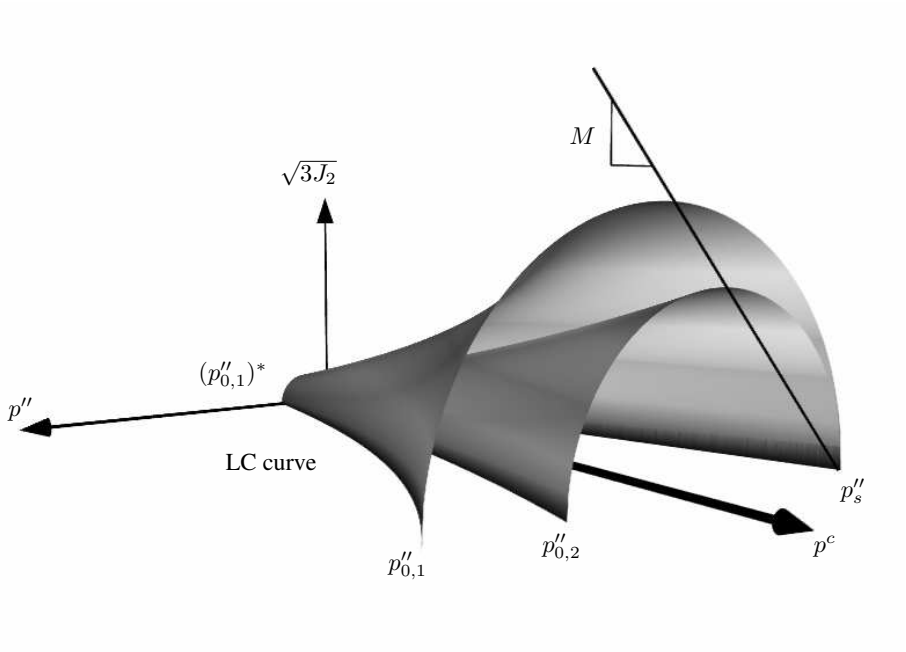

Figure 1: Yield surface of the BBM for different values of the preconsolidation pressure

with the flow potential

$$g = \alpha J_2 - \frac{M^2}{3}\left(p'' + p''_s\right)\left(p''_0 - p''\right) \ , \tag{10}$$

where α is a constant. The hardening law relates the rate of the preconsolidation pressure at saturated conditions $(p''_0)^*$, which serves as the hardening parameter, to the volumetric plastic strain rate $\dot{\varepsilon}^p_v$ by

$$(\dot{p}''_0)^* = (p''_0)^* \frac{1+e}{\lambda(0)-\kappa}\dot{\varepsilon}^p_v \ . \tag{11}$$

(11) describes the evolution of the yield surface. The latter is shown for two different values of $(p''_0)^*$ in Fig. 1.

3 AN OPTIMIZED RETURN MAPPING ALGORITHM

For deriving a computationally efficient version of the return mapping algorithm the flow rule (9) is split into a volumetric and deviatoric part

$$\dot{\varepsilon}^p_v = \dot{\gamma}\ 3\frac{\partial g}{\partial I''_1} \ , \qquad \dot{e}^p_{ij} = \dot{\gamma}\frac{\partial g}{\partial J_2} s_{ij} \ . \tag{12}$$

Backward Euler integration of (12) yields

$$\begin{aligned} \Delta\varepsilon_v^p &= \gamma\ 3\frac{\partial g}{\partial I_1''} = \Delta\varepsilon_v - \Delta\varepsilon_v^e\ , \\ \Delta e_{ij}^p &= \gamma\frac{\partial g}{\partial J_2}s_{ij} = \Delta e_{ij} - \Delta e_{ij}^e\ , \end{aligned} \tag{13}$$

where $\gamma = \dot{\gamma}\Delta t$. Note that quantities with the subscript n refer to the converged values at the previous time instant t_n, whereas all other quantities refer to the values at the current time instant t_{n+1}. In case of a constant value of G

$$\begin{aligned} s_{ij} = 2Ge_{ij}^e &= 2G\left[(e_{ij} - e_{ij,n}^p) - (e_{ij}^p - e_{ij,n}^p)\right] \\ &= s_{ij}^{Trial} - 2G\Delta e_{ij}^p \end{aligned} \tag{14}$$

follows from (3_2). Inserting (13) into (14) gives

$$\left(1 + \gamma\frac{\partial g}{\partial J_2}2G\right)s_{ij} = s_{ij}^{Trial}\ . \tag{15}$$

The term enclosed by the brackets is a scalar quantity, hence, s_{ij} and s_{ij}^{Trial} differ only by a scalar factor. Thus, from (15) it follows

$$\left(1 + \gamma\frac{\partial g}{\partial J_2}2G\right)^2 J_2 = J_2^{Trial}\ . \tag{16}$$

Making use of $\gamma = (\Delta\varepsilon_v - \Delta\varepsilon_v^e)/(3\partial g/\partial I_1'')$, resulting from ($13_1$), yields

$$\left(3\frac{\partial g}{\partial I_1''} - \frac{\partial g}{\partial J_2}2G(\Delta\varepsilon_v^e - \Delta\varepsilon_v)\right)^2 J_2 - \left(3\frac{\partial g}{\partial I_1''}\right)^2 J_2^{Trial} = 0\ . \tag{17}$$

In (17) the incremental volumetric strain $\Delta\varepsilon_v$ is known from the current estimate of the displacement increment at t_{n+1}. J_2 and $\Delta\varepsilon_v^e$ in (17) can be replaced by

$$J_2 = \frac{M^2}{3}\left(p'' + p_s''\right)\left(p_0'' - p''\right) \tag{18}$$

and

$$\Delta\varepsilon_v^e = \frac{\kappa}{1+e}\ln\left(\frac{p''}{p_n''}\right) + \frac{\kappa_s}{1+e}\ln\left(\frac{p^c + p_{atm}}{p_n^c + p_{atm}}\right) \tag{19}$$

following from (7) and from integration of the rate constitutive equation (3_1). The rate of the void ratio is given by

$$\dot{e} = -(1+e)\,\dot{\varepsilon}_v\ . \tag{20}$$

Integration of (20) yields the value of the void ratio at t_{n+1}

$$e = (1+e_n)\exp(-\Delta\varepsilon_v) - 1\ . \tag{21}$$

(17) together with (18), (19), (21) and (6) represents a nonlinear scalar equation for the unknown I_1'' (or $p'' = I_1''/3$), which can be solved, e.g., by the Newton method. Once p'' has been determined from this equation, it is inserted into (6), yielding p_0'', and the latter into the recast form of (8_2) yielding the hardening parameter $(p_0'')^*$.

4 COMPARISON OF DIFFERENT STRESS UPDATE ALGORITHMS

To investigate the performance of the proposed stress update algorithm, the following stress update algorithms are considered in the subsequent comparative study:

(a) an explicit stress update algorithm, characterized by forward integration of the constitutive rate equation

$$\dot{\boldsymbol{\sigma}} = \mathbb{C}^{ep}\dot{\boldsymbol{\varepsilon}} + \mathbf{C}^{p^c,ep}\dot{p}^c \tag{22}$$

with $\mathbb{C}^{ep} = \partial\boldsymbol{\sigma}/\partial\boldsymbol{\varepsilon}$ and $\mathbf{C}^{p^c,ep} = \partial\boldsymbol{\sigma}/\partial p^c$ denoting the constitutive tangent operators, which is combined with adaptive sub-stepping and error control based on the Richardson extrapolation method;

(b) a general return mapping algorithm [13], characterized by backward Euler integration of the rate equations for the plastic strains (9) and the hardening variable (11) and by enforcing the condition $f = 0$ for the yield function (7) at t_{n+1}, which requires solving a system of nonlinear equations, consisting of the consistency parameter, the net stress and the hardening variable;

(c) the optimized return mapping algorithm described in section 3 and [6] respectively;

(d) a semi-explicit stress update algorithm [10], characterized by explicit integration of the rate equations for the plastic strains (9) and the hardening variable (11) and by enforcing the condition $f = 0$ for the yield function (7) at t_{n+1} for determining the consistency parameter, which is combined with adaptive sub-stepping and error control based on the Richardson extrapolation method;

(e) the implicit fifth-order Runge–Kutta integration algorithm with error control RADAU5, proposed in [4].

A comparison of the investigated stress update algorithms with respect to the accuracy is performed on the basis of two different sets of material parameters for the BBM, provided in [1]. To this end, the error of the stresses computed for prescribed combinations of volumetric and deviatoric strain increments are considered. The error is defined as a relative error, related to the "exact" value for the respective stress component computed by the RADAU5 algorithm [4] prescribing an extremely small error tolerance of 10^{-10}.

Fig. 2 shows a comparison of the integration errors obtained by means of the general return mapping algorithm and the optimized return mapping algorithm for the relatively large range of strain increments ranging from 0 up to 3%. A particular point of the diagrams shown in Fig. 2 indicates the error of a single step stress update for a particular combination of volumetric and deviatoric strain increment $(\varepsilon_v, \varepsilon_s)$. E.g., the point $(\varepsilon_v = 2\%, \varepsilon_s = 3\%)$ represents the integration error for the strain increment $\Delta\varepsilon_v = 0.02$ and $\Delta\varepsilon_s = 0.03$, obtained by a single step backward Euler integration. According to Fig. 2 the integration errors for the investigated strain increments reach up to 40%. Contrary

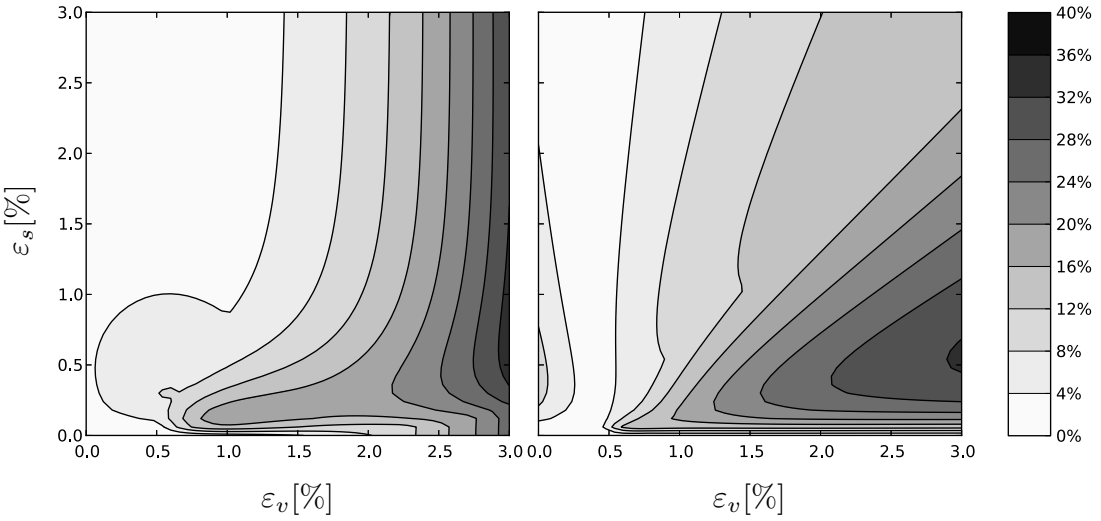

Figure 2: Integration errors for the general return mapping algorithm (left) and the optimized return mapping algorithm (right)

to the general return mapping algorithm the optimized return mapping algorithm gives the exact solution for hydrostatic strain paths due to the analytical integration of the hardening law. Because of the large integration errors, similar to the explicit and semi-explicit stress update algorithm, the return mapping algorithms are also enhanced by adaptive sub-stepping and error control.

For the investigation of the efficiency of the considered stress update algorithms the stresses were computed for 25 combinations of volumetric and deviatoric strain increments of 0.5%, 0.75%, 1.0%, 1.25% and 1.5% for prescribed maximum values of the integration error, ranging from 10^{-1} to 10^{-10}. The mean values of the number of required instructions are shown in the diagrams of Fig. 3 for the resulting mean values of the computed errors.

It follows from Fig. 3 that for a prescribed error tolerance the optimized return mapping algorithm is by far more efficient than the general return mapping algorithm and it is even more efficient than the explicit integration method. The RADAU5 algorithm is very efficient for very small prescribed values of error tolerances.

5 APPLICATION TO A COUPLED FINITE ELEMENT ANALYSIS

The application of the developed optimized return mapping algorithm is demonstrated by a coupled solid-fluid Finite Element analysis of the water flow through a homogeneous earth dam. The cross section of the homogeneous earth dam is shown in Fig. 4, the employed hydraulic parameters and material parameters are reported in [11, 12]. A rigid foundation of the dam is assumed by constraining the displacements on the bottom of the dam. For the undrained part of the base an impermeable boundary is assumed, whereas for the drained part a permeable boundary is considered by applying a mass flux with a

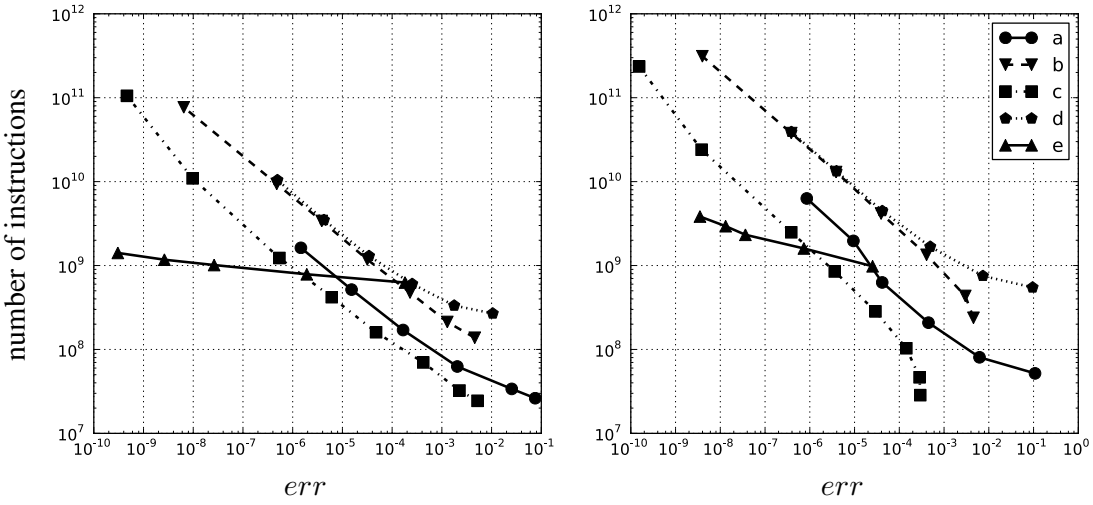

Figure 3: Work precision diagrams for two sets of material parameters: (a) explicit stress update, (b) general return mapping algorithm, (c) optimized return mapping algorithm, (d) semi-explicit stress update algorithm, (e) implicit fifth-order Runge–Kutta algorithm

pressure dependent velocity

$$\begin{aligned} v_n &= k_{sc}\, p^w \quad \text{for} \quad p^w > 0, \\ v_n &= 0 \quad \text{for} \quad p^w \leq 0, \end{aligned} \tag{23}$$

with p^w denoting the water pressure at the boundary and k_{sc} is a sufficiently large seepage coefficient to approximately enforce the requirement of a zero water pressure for a freely draining surface. Similar boundary conditions for the fluid phase are applied at the free surfaces, i.e. at the upstream slope above the water level, the crest and the downstream slope.

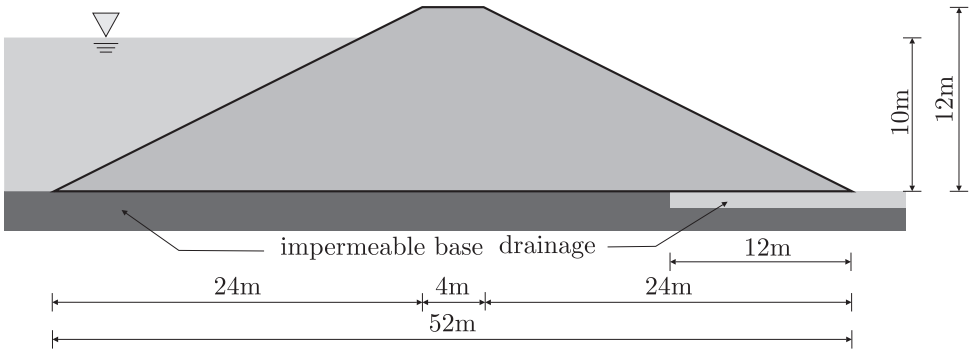

Figure 4: Cross section of the homogeneous earth dam

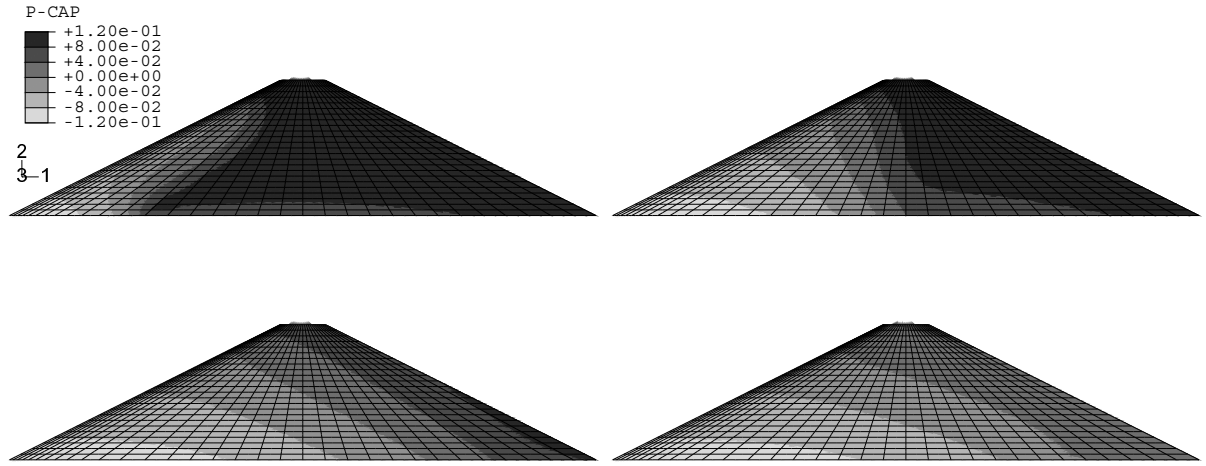

Figure 5: Distribution of matric suction for selected time instants from top to bottom: (a) t = 20 d, (b) t = 60 d, (c) t = 310 d, (d) t = 800 d

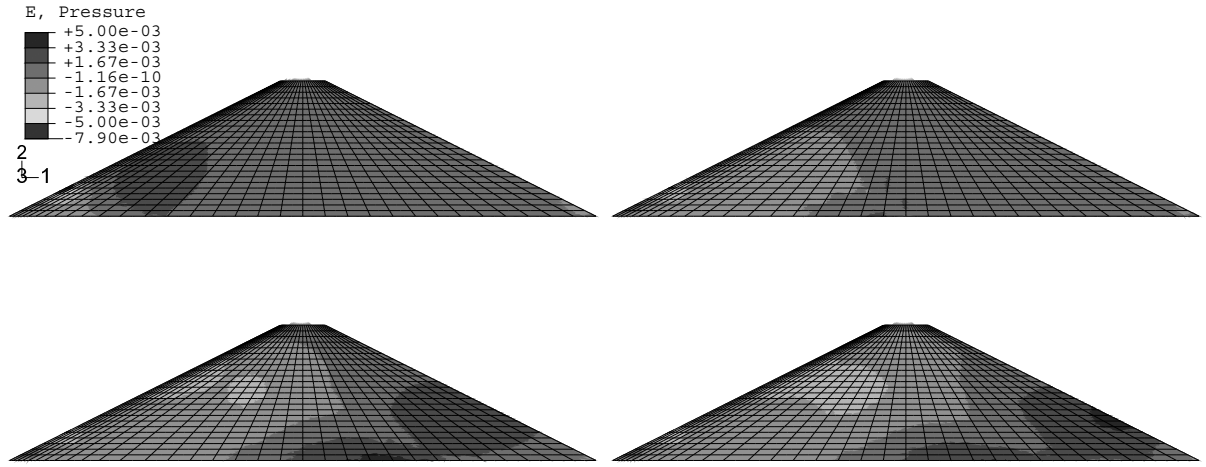

Figure 6: Distribution of the volumetric strain for selected time instants: t = 20 d, t = 60 d, t = 310 d, t = 800 d

In the first step of the numerical analysis a constant matric suction of 100 kPa, corresponding to an initial degree of water saturation of $S^w = 0.729$, is assumed for the dam body and the primary stresses due to dead load are computed presuming elastic response. In the second step the net stresses, the void ratio and matric suction, computed in the first step, are taken as initial values, whereas the displacements are set equal to zero and matric suction at the upstream boundary is reduced to zero by specifying the respective boundary conditions. In the subsequent steps of the analysis the transient seepage flow

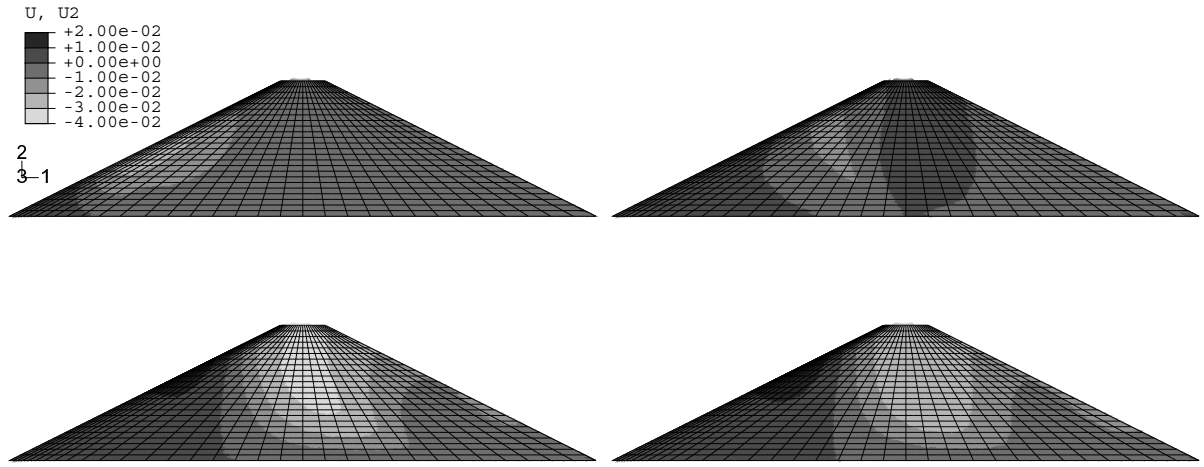

Figure 7: Vertical displacements for selected points of time from top to bottom: (a) t = 20 d, (b) t = 60 d, (c) t = 310 d, (d) t = 800 d

due to a water table of $H = 10\ m$ is computed until steady state conditions are attained.

Figure 5 shows the distribution of matric suction for selected time instants. Negative values of matric suction represent values of the water pressure in fully water saturated regions. 20 days after impoundment only a small region close to the upstream slope is affected by the water flow. With advancing time the water saturated domain is propagating until steady state conditions are attained.

The distribution of the volumetric strain with advancing saturation front is shown in Fig. 6. Volumetric compaction, indicated by positive values of the volumetric strain, occurs in the lower central region and in the downstream regions which are characterized by partial saturation. The computed distribution of the vertical displacements of the soil skeleton (negative values denote settlements) is shown in Figure 7. Shortly after the impoundment settlements in the vicinity of the upstream face of the dam occur, whereas at later stages uplifting is predicted in this region. By contrast, in the upper central region of the dam, the settlements increase with advancing saturation front.

6 CONCLUSIONS

In this paper an optimized return mapping algorithm was proposed, which is characterized by analytical integration of the hardening law and by solving only a nonlinear scalar equation at the integration point level. To investigate the performance of the developed algorithm, several stress update algorithms were compared with respect to accuracy and efficiency: (a) an explicit stress update algorithm, (b) a general return mapping algorithm, (c) the proposed optimized return mapping algorithm, (d) a semi-explicit stress update algorithm, and (e) an implicit fifth-order Runge-Kutta stress update algorithm. Large integration errors were encountered for the return mapping algorithms when larger

strain increments were integrated in one step. Hence, similar to the explicit and semi-explicit stress update algorithm, they were enhanced by adaptive sub-stepping and error control. It was shown that for a prescribed error threshold value the optimized return mapping algorithm is by far more efficient than the general return mapping algorithm and it is even more efficient than the explicit integration method. Finally, to demonstrate the robustness and efficiency of the proposed algorithm within a Finite Element context, a simplified 2D coupled transient numerical simulation of the behavior of an embankment dam due to impoundment was performed.

References

[1] Alonso, E. E., A. Gens, and A. Josa (1990). A constitutive model for partially saturated soils. *Géotechnique 40*, 405–430.

[2] Cui, Y. J., P. Delage, and N. Sultan (1995). An elasto-plastic model for compacted soils. In *Unsaturated soils*, Volume 2, pp. 703–709. Balkema, Rotterdam.

[3] Fellin, W., M. Mittendorfer, and A. Ostermann (2009). Adaptive integration of constitutive rate equations. *Computers and Geotechnics 36*(5), 698–708.

[4] Hairer, E. and G. Wanner (1996). *Solving Ordinary Differential Equations II, Stiff and Differential-Algebraic Problems* (2^{nd} rev. ed.). Springer Berlin Heidelberg.

[5] Hickman, R. J. and M. Gutierrez (2005). An internally consistent integration method for critical state models. *International Journal for Numerical and Analytical Methods in Geomechanics 29*(3), 227–248.

[6] Hofmann, M. (2010). *Integrationsalgorithmen und Parameteridentifikation elasto-plastischer Stoffgesetze f"ur teilges"attigte Materialien.* Ph. D. thesis, Universit"at Innsbruck.

[7] Josa, A., A. Balmaceda, A. Gens, and E. E. Alonso (1992). An elastoplastic model for partially saturated soil exhibiting a maximum of collapse. In *3rd international conference on computational plasticity*, Volume 1, Barcelona, pp. 815–826.

[8] Lewis, R. W. and B. A. Schrefler (1998). *The Finite Element Method in the Static and Dynamic Deformation and Consolidation of Porous Media* (2 ed.). John Wiley & Sons.

[9] Marie Curie Research Training Network (2009). http://muse.dur.ac.uk. (April 17, 2009).

[10] Mittendorfer, M. (2006). Interne Differentiation nichtlinearer anelastischer Materialmodelle. Master's thesis, Leopold-Franzens-Universität Innsbruck.

[11] Pertl, M. (2010). *Grundlagen, Implementierung und Anwendung eines Drei-Phasen Modells für Böden*. Ph. D. thesis, Universität Innsbruck.

[12] Pertl, M., M. Hofmann, and G. Hofstetter (2011). Coupled solid-fluid fe-analysis of an embankment dam. *Frontiers of architicture and civil engineering in China 5*(1), 53–62.

[13] Simo, J. and T. Hughes (1998). *Computational Inelasticity*. Springer New York.

[14] Wheeler, S. J. and V. Sivakumar (1995). An elasto-plastic critical state framework for unsaturated soil. *Géotechnique 45*, 35–53.